Catalysis Today 165 (2011) 10–18

Contents lists available at ScienceDirect

Catalysis Today

journal homepage: www.elsevier.com/locate/cattod

Adsorption and activation of CO_2 over the Cu–Co catalyst supported on partially hydroxylated γ-Al_2O_3

Shuxia Yin, Todd Swift [1], Qingfeng Ge*

Department of Chemistry and Biochemistry, Southern Illinois University, 1245 Lincoln Drive, Carbondale, IL 62901, United States

ARTICLE INFO

Article history:
Available online 11 January 2011

Keywords:
CO_2 adsorption and activation
Bimetallic catalyst
Support effect
Density functional theory

ABSTRACT

A multi-component catalyst offers an opportunity to regulate the conversion of CO_2 toward the desired product through the synergistic effect of different active components. Herein, the effect of incorporating Cu into a cobalt-based cluster, supported on the partially hydroxylated γ-Al_2O_3 (1 1 0) surface, on CO_2 adsorption has been studied using periodic density functional theory calculations. Three CO_2 adsorption modes were identified on these Co–Cu bimetallic clusters: (a) CO_2 symmetrically binds the bridge site of the metals through mixed carbon/oxygen coordination with the metal atoms; (b) CO_2 asymmetrically adsorbs at the interfacial site via carbon/oxygen–metal coordination and hydrogen bonding to the surface hydroxyl; and (c) protonated CO_2 at the interface. The incorporation of Cu into a cobalt-based cluster reduces the binding strength of the adsorbed CO_2 and changes the favorable site of CO_2 adsorption: the most favorable adsorption site for CO_2 adsorption changes from the bridge site of the Co_4 cluster to the interfacial sites of the Co_3Cu and $CoCu_3$ clusters. The interfacial structure is stabilized by hydrogen bonding with the surface hydroxyl group, resulting in an asymmetrically activated CO_2 adsorption complex. This complex may be hydrogenated directly by the co-adsorbed hydrogen atoms, leading to the oxygenate products.

1. Introduction

Catalytic conversion of carbon dioxide has gained increasing attention in recent years as it provides a promising way to utilize the unlimited source of CO_2 to produce valuable chemicals within the current energy infrastructure as well as contribute to reducing net CO_2 emission to the atmosphere [1,2]. Transition metal catalysts supported on a range of metal oxides have been studied in the catalytic CO_2 conversion by reacting with H_2 or natural gas. The conversion products, ranging from methane or methanol to long chain hydrocarbons, are determined by the type and nature of catalysts as well as reaction conditions, such as feedstock ratio and pressures. Many studies have been focused on discovering catalysts with high activity and selectivity toward the desired products [3–17]. Catalysts with a second metal as a cocatalyst or promoter are common for CO_2 activation and conversion. In these multi-component catalysts, the arrangement of atoms and the interfacial properties can be controlled to optimize the activity and selectivity of the catalytic process. On the other hand, due to the complexity of the reaction occurring on multi-component catalysts, an understanding of the catalytic mechanism at the atomic level cannot be easily achieved. Herein, we present a theoretical investigation on the adsorption and activation of CO_2 over a bimetallic cluster supported on the hydroxylated alumina surface. We hoped to provide some insights into the effect of introducing a second metal on the reactivity of the catalyst as well as its implication for the ultimate selectivity.

Cu-based catalysts dispersed on oxides, such as γ-Al_2O_3, SiO_2 and ZrO_2, have been widely studied for CO_2 hydrogenation, to produce methanol, and reforming CH_4, to produce synthesis gas [6–12]. Furthermore, CO_2 has been co-fed with CO and H_2 in producing hydrocarbon through Fischer–Tropsch (F–T) synthesis. Both Co- and Fe-based catalysts have been explored for F–T synthesis in the presence of CO_2 [13–17]. Early studies reported a promotion effect of Cu to F–T rate on the Fe-based catalyst [18–20], manifested as the addition of Cu to the Fe catalyst enhancing the rate of the iron oxide reduction and resulting in a more active catalyst. The promotion effect of Cu for CO_2 hydrogenation through F–T synthesis has been observed by Iglesia's group [14] on the Fe–Zn catalysts. Lee and his coworker also studied CO_2 conversion and selectivity of Fe–Cu–K catalyst on the supports including Al_2O_3, SiO_2 and TiO_2 as well as the metal structural promoters such as V, Cr, Mn and Zn [15]. They confirmed the Cu and K promotion effect and found that Al_2O_3 as a support enhances CO_2 chemisorption. They showed that the addition of Cr, Mn and Zn generated more basic sites and increase the selectivity toward C_2–C_4, and among which Zn gives the highest selectivity. On the contrary, the pres-

* Corresponding author. Tel.: +1 618 453 6406; fax: +1 618 453 6408.
E-mail address: qge@chem.siu.edu (Q. Ge).
[1] REU student from Case Western Reserve University.

0920-5861/$ – see front matter © 2010 Elsevier B.V. All rights reserved.
doi:10.1016/j.cattod.2010.12.025

ence of Cu in the Co catalyst was found to reduce the rate of F–T synthesis in an early study [18]. Very recently, Jacobs et al. have reported an EXAFS study on the Cu promoted Co/Al_2O_3 F–T catalyst [21]. They observed that although adding Cu facilitates Co reduction, the increased fraction of reduced Co did not lead to a higher density of active sites because Cu tends to cover the rim of Co clusters, which reduces the CO conversion rate and causes the selectivity to the light components to increase. On the other hand, the addition of a small amount of noble metal to the supported Co catalyst in F–T synthesis [22–26] resulted in an increased catalytic activity. Dorner et al. investigated the hydrogenation of CO_2 on the $Co–Pt/Al_2O_3$ catalyst [17]. These authors reported that the predominant product was methane, with a small fraction of longer chain hydrocarbons being produced as the pressures and H_2/CO_2 ratios in the feed decrease. The increased hydrogenation rate in the presence of Pt was attributed to the increase of the reduced Co whereas the change of the product distribution was attributed to the presence of other active sites on the surface.

Generally, the processes of CO_2 conversion are regulated by many factors, including catalyst/co-catalyst, supporting oxides, promoters as well as reaction environment. In particular, the structure of the metal catalyst on the support can be modified by varying the ratio of the active components, which in turn influences the density and distribution of the active sites for adsorption of CO_2 and the reaction intermediates. Despite so many investigations of multi-component catalysts, the function of catalytic metals as well as the reaction pathway is still ambiguous. Therefore understanding CO_2–metal interactions and the synergy of metal-support and metal components at catalyst–oxide interfaces is key to resolving the complex catalytic process and achieving rational catalyst design. There are a few theoretical studies on CO_2–catalyst or CO_2-crystal surface interactions [27–33] whereas even few studies on the mechanism of the catalyst reactivity regulated by the catalyst composition change. Here we made an attempt to study CO_2 adsorption on a model bimetallic catalyst supported on an alumina surface and tried to understand the role of catalyst composition tuning on CO_2 conversion.

Focusing on the atomic level detail of CO_2–cluster–support interfacial interaction, we report a periodic density functional theory study of CO_2 adsorption and activation on Co–Cu bimetallic clusters supported on γ-Al_2O_3 (1 1 0) surface, with Co/Cu ratio variation. As mentioned above, copper is much less active than cobalt and reduces the rate of F–T synthesis when used as a promoter [18]. However, as a commonly used catalyst for methanol, it may increase the selectivity toward methanol. These two effects may produce a synergy in the catalyst based on the two metals. Experimentally, γ-alumina has been widely used as a support for many heterogeneous catalysts, due to its high porosity and the presence of acid and base sites, and availability [34]. Additionally, it is observed to increase CO_2 adsorption [15]. Here we selected a tetramer bimetallic cluster of Co and Cu supported on γ-Al_2O_3 to explore the CO_2 adsorption at cluster–support interface. The comparative studies of CO_2 on clusters with different Cu/Co ratios demonstrate that the active sites for CO_2 adsorption can shift by tuning the metal composition, which in turn affects the reaction energetics and leads to a change in the product distribution.

2. Computational details

Density functional theory periodic slab calculations were carried out using the Vienna ab initio simulation package (VASP) [35–37]. The projector augmented wave method was employed to describe the interactions between ion and electrons [38]. The exchange and correlation energy was evaluated using the Perdew–Burke–Ernzehof (PBE) form of the generalized gradient approximation (GGA) functional [39]. The cutoff energy for the plane wave basis set was set to 400 eV. The Brillouin zone integration was performed with the k points generated from $2 \times 2 \times 1$ Monkhorst–Pack grid [40]. The atomic structures were optimized using the conjugated gradient algorithm and/or the quasi-Newton scheme until the forces on the unconstrained atoms were less than 0.03 eV/Å. Spin-polarization was included in all our calculations to account for the magnetic nature of Co.

We adopted the model of the partially hydroxylated γ-Al_2O_3 (1 1 0) surface based on our previous studies [30–32]. The supercell includes twelve Al_2O_3 units distributed in six layers and a 12 Å vacuum, and has a dimension of $8.404\,Å \times 8.018\,Å \times 19.182\,Å$. In the surface unit cell, one H_2O molecule dissociates into a hydroxyl occupying a three-coordinated Al site and a proton binding a neighboring two-coordinated O site. Consequently, there are two hydroxyls produced in each surface unit cell, corresponding to a OH coverage of $\sim$3 OH/nm^2. In all calculations, the bottom two layers were fixed at their bulk positions whereas the top four layers as well as the adsorbed clusters, hydroxyls and CO_2 were allowed to relax. The binding of Co_3Cu and $CoCu_3$ clusters on the above hydroxylated surface were first explored in both planar and tetrahedral configurations. CO_2 was then added to the supported cluster. Bader-charge analysis was used to characterize the stable structural configurations [41,42]. The adsorption energy of CO_2 is defined as:

$$\Delta E_{ad} = E_{CO_2-cluster/\gamma\text{-}Al_2O_3} - E_{cluster/\gamma\text{-}Al_2O_3} - E_{CO_2}$$

where $E_{CO_2-cluster/\gamma\text{-}Al_2O_3}$, $E_{cluster/\gamma\text{-}Al_2O_3}$ and E_{CO_2} are the total energies of the slab with adsorbed cluster and CO_2, the slab with only cluster adsorbed, and the isolated CO_2 molecule, respectively. A more negative adsorption energy corresponds to a stronger binding of CO_2 on the supported cluster.

Constant-temperature (300 K and 500 K) ab initio molecular dynamics simulations with similar parameters to those used in geometry optimization have been performed for adsorbed CO_2. In the dynamics run, we reduced the cutoff energy to 300 eV to reduce the computational costs. The time step was set at 0.5 fs and the simulation ran up to 2.5 ps. The most stable adsorption configurations of CO_2 on supported clusters obtained from the static relaxation were selected as the initial configuration for the dynamic runs.

3. Results and discussion

3.1. Bi-metallic cluster supported on hydroxylated γ-Al_2O_3 (1 1 0) surface

To shed light on the effect of Cu incorporation, CO_2 adsorption on a pure cobalt cluster Co_4 has been conducted. The bimetallic clusters, Co_3Cu and $CoCu_3$, as well as Co_4 were modeled in both tetrahedral and planar configurations. The tetrahedral configuration is less favorable energetically than the planar one in the gas phase. Upon binding on the hydroxylated γ-Al_2O_3 (1 1 0) surface, the tetrahedral configuration shows a stronger interaction. We therefore focused our attention on the tetrahedral configuration in the present study. The adsorption of the cluster was explored on a number of surface sites. The most favorable configurations are shown in Fig. 1(a–c), named as T_{Co_3Cu} for adsorbed Co_3Cu cluster, T_{Cu_3Co} for Cu_3Co and T_{Co_4} for Co_4. The clusters are located above surface Al_{4c}, O_{2c}, O_{3c1}, and O_{3c2} sites, with Co/Cu binding these sites and the basal plane of the tetrahedron lying slantingly on the surface. The O_{3c2} site is less active than the O_{2c} site, indicated by the fact that the adsorbed cluster shifted toward the O_{2c} and O_{3c1} sites after relaxation. Overall, the binding sites are similar for both clusters, while the local coordination and electronic structure differ. These differences are crucial to better understand adsorption and activation of CO_2 over the supported catalysts.

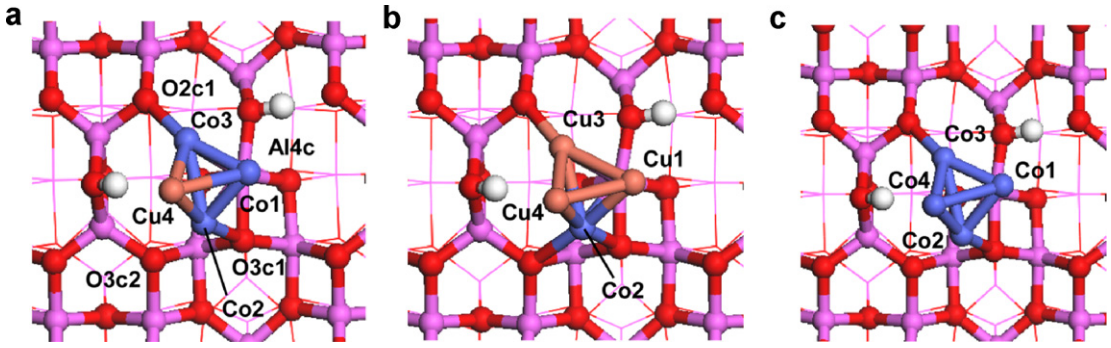

Fig. 1. Top view of the metal clusters supported on the partially hydroxylated γ-Al_2O_3 (1 1 0) surface: (a) T_{Co_3Cu}; (b) T_{CoCu_3}; (c) T_{Co_4}. Red, O; pink, Al; blue, Co; light brown, Cu; gray, C; and white, H. (For interpretation of the references to color in this figure legend, the reader is referred to the web version of the article.)

In T_{Co_3Cu} (Fig. 1a), three Co atoms interact with the surface directly, forming Co_3–O_{2c}, Co_2–O_{3c1} and three Co–Al_{4c} bonds, whereas Cu is located at the top vertex away from the support surface. Detailed analyses of Cu substitution of Co in different positions showed that cobalt energetically favors the surface sites more than copper, leading to copper at the tetrahedral vertex of the cluster being the most favorable. The overall binding strength of the cluster decreases with the Cu position in the order of vertex site, Al_{4c}, O_{2c} and O_{3c1}.

The discernible coordination of Co and Cu with the surface can be understood by considering the surface acidic/basic sites and the electron donating ability of Co and Cu. The electronegativities of Cu, Co and Al are 1.90, 1.88, and 1.60 eV, respectively. These values indicate that Co has a higher electron donating ability than Cu, as clearly reflected in the isolated Co_3Cu cluster, in which Cu is negatively charged (Table 1). Therefore, Co interacts more strongly with the surface basic sites than Cu does. Bader charges in Table 1 also show that the Co atoms bound with the surface O site are positively charged, clearly indicating the cationic nature of Co when interacting with a basis site. In contrast, the Co atom binding Al_{4c} and the Cu atom in the top vertex are negatively charged, suggesting electron redistribution when the cluster is adsorbed on surface. The Co atom became more negative, due to its interaction with the acidic Al_{4c} site. The adsorbed cluster has a net positive charge, indicating an electron transfer from the cluster to the surface.

When more Co atoms are replaced by Cu, the substitution is expected to occur at the sites in the order of decreasing binding strength, i.e., top vertex site, Al_{4c}, O_{2c}, and O_{3c1}. For T_{Co_3Cu} (Fig. 1b), the Cu substitution occurred at the first three sites and the lone Co remains binding the O_{3c1} site. Bader charge analysis shows that the Cu atom binding the Al_{4c} site and the Cu atom in the top vertex are negatively charged, similar to those in the T_{Co_3Cu} case. As shown in Table 1, the adsorbed cluster has a smaller positive charge, indicating a weaker electron transfer from the cluster to the surface after Co was substituted by Cu.

The more significant electron transfer between the Co_3Cu cluster and surface relative to that of $CoCu_3$ cluster corresponds to a stronger Co_3Cu–surface interaction than the $CoCu_3$–surface interaction. The adsorption energy of Co_3Cu is −3.69 eV with respect to the hydroxylated surface and free cluster, and is more favorable by 0.29 eV than $CoCu_3$ adsorption. From Co_4 to Co_3Cu and multi-substituted $CoCu_3$, the electron transfer to the substrate surface decreases with the increased substitution. We therefore conclude that Cu incorporation decreases the electron donating ability of the clusters.

The above analyses demonstrated that the cluster–surface interaction is determined by distribution and availability of the surface acid–basic sites as well as the nature of the metal atoms. The structural differences of these supported clusters are expected to affect their activity as catalysts for CO_2 adsorption and further reactions. In the following sections, we examine CO_2 adsorption on the two bimetallic clusters and compare with that on the Co_4 cluster. The change in catalytic property by tuning the composition will be discussed in the context of CO_2 activation.

3.2. CO_2 adsorption on supported bi-metallic clusters

We explored CO_2 adsorption on T_{Co_3Cu} and T_{CoCu_3} as well as T_{Co_4} systematically. In all stable configurations, the adsorbed CO_2 is bent, indicating it is activated. The activation of CO_2 in the adsorbed state results in a charged CO_2 species, represented as CO_2^-. CO_2 binds the cluster via mixed oxygen/carbon coordination with the cluster Co or Cu atoms, or at the cluster–surface interface through the oxygen/carbon coordination with cluster and the surface hydroxyl O_s and Al_{4c}. Accordingly, the configurations of the adsorbed CO_2 can be classified into three modes. Mode 1 only involves CO_2 and the metal cluster. The adsorbed CO_2 is distorted quasi-symmetrically and bound at a metal–metal bridge site by coordinating with two metal atoms, thus Mode 1 is also referred to as bridge mode. Mode 2 involves both metal cluster and the supporting oxide. The adsorbed CO_2 is distorted asymmetrically and coordinated with one or two metal atoms at the cluster–support interface. Moreover, the adsorbed CO_2 are stabilized by forming a hydrogen bond with the surface hydroxyl group or by direct

Table 1
Bader charges (e) and adsorption energies (eV) for bimetallic clusters supported on the partially hydroxylated γ-Al_2O_3 (1 1 0) surface.

	Co_4			Co_3Cu			$CoCu_3$		
		Isolated	T_{Co_4}		Isolated	T_{Co_3Cu}		Isolated	T_{CoCu_3}
Atomic bader charge	Co[a]	0.05	−0.27	Co[a]	0.06	−0.25	Co	0.04	0.04
	Co	−0.03	0.30	Co	0.04	0.29	Cu[a]	−0.02	−0.07
	Co	0.00	0.30	Co	0.06	0.32	Cu	0.00	0.23
	Co[b]	−0.02	−0.13	Cu[b]	−0.16	−0.21	Cu[b]	−0.02	−0.13
Net bader charge		0.0	0.19		0.0	0.15		0.0	0.07
$\Delta E_{ad}^{cluster}$			−3.04			−3.69			−3.40

[a] Corresponding to atoms binding Al_{4c}.
[b] The top vertex atom.

Table 2
Adsorption energies and structural parameters of CO_2 adsorbed on the γ-Al_2O_3 supported Co_3Cu cluster in different configurations (^{s} labels the surface atom).

		ΔE_{ad} (eV)	$O^{a(b)}$…H–O^s (Å)	Adsorption site	C–O^a, C–O^b (Å)	∠O–C–O(°)
Mode 1	A1_1	−0.61	No	Co_1–Cu_4	1.24, 1.26	142.5
Mode 2	A2_1	−0.85	1.64	Co_1–Co_2	1.23, 1.33	131.7
	A2_2	−0.82	1.62	Co_1	1.21, 1.32	137.8
	A2_2′	−0.61	No	Co_1	1.21, 1.28	142.9
	A2_3	−0.88	1.62	Co_1–Co_2, Al_{4c}	1.22, 1.44	123.9
	A2_4	−0.83	1.68	Co_1	1.21, 1.29	139.8
	A2_5	−0.69	1.56	Co_1	1.20, 1.32	137.5
Mode 3	A3_1	−1.34	1.65	Protonated	1.29, 1.33	115.1
	A3_2	−1.39	1.49	Protonated	1.41, 1.27	118.9
	A3_3	−0.62	1.62	Protonated	1.22, 1.35	123.1

Note: the apostrophe in the notation A2_2′ means the structure is same as A2_2 except without hydrogen bonding formation.

Table 3
Adsorption energies and structural parameters of different CO_2 adsorption configurations on γ-Al_2O_3 supported $CoCu_3$.

		ΔE_{ad}(eV)	$O^{a(b)}$…H–O^s (Å)	Adsorption site	C–O^a, C–O^b (Å)	∠O–C–O (°)
Mode 1	B1_1	−0.68	No	Co_2–Cu_4	1.26, 1.26	137.2
Mode 2	B2_1	−1.04	1.62	Cu_1–Co_4	1.24, 1.31	131.9
	B2_2	−0.46	1.53	Cu_1	1.25, 1.23	139.1
	B2_3	−0.11	1.66	Cu_1	1.20, 1.29	139.6
	B2_4	−0.42	1.55	Cu_4	1.23, 1.23	142.0
Mode 3	B3_1	−1.24	1.57	Protonated	1.29, 1.32	114.9
	B3_2	−1.70	1.47	Protonated	1.39, 1.26	118.4

Table 4
Bader charges (e) on adsorbed CO_2 and the clusters in different configurations.

		On T_{Co_3Cu}			On T_{CoCu_3}	
		CO_2	Cluster		CO_2	cluster
Mode 1	A1_1	−0.99	0.78	B1_1	−0.73	0.76
Mode 2	A2_1	−0.86	0.83	B2_1	−0.79	0.75
	A2_2	−0.67	0.65	B2_2	−0.59	0.54
	A2_3	−1.13	1.00	B2_3	−0.58	0.63
	A2_4	−0.63	0.60	B2_4	−0.52	0.48
Mode 3	A3_1	−1.30	1.18	B3_1	−1.26	1.10
	A3_2	−1.33	1.16	B3_2	−1.22	1.04
	A3_3	−0.93	0.88			

interaction of the O atom with surface Al_{4c} atom. This mode is referred to as the interface mode. Mode 2 can be further divided into single-metal and bi-metal coordination, based on CO_2–cluster coordination. Mode 3, referred to as the protonated mode, is also formed at the cluster–support interface. In these configurations, the adsorbed CO_2 is further protonated by the surface OH group through a proton transfer process. In the following presentation, the adsorption configurations on T_{Co_3Cu} are denoted as A_1, A_2 and A_3, according to their coordination modes, and on T_{CoCu_3} as B_1, B_2 and B_3, and on T_{Co_4} as O_1, O_2, and O_3. When there is a need to distinguish local minima, we add an additional number to the subscript. For example, A_{2_1} and A_{2_2} represent the two configurations of Mode 2 on T_{Co_3Cu}. The two oxygen atoms of CO_2 are labeled as O_a and O_b when they are in unequivalent positions and the oxygen of surface hydroxyl is marked as O_s. All the structural parameters and adsorption energies for these configurations are summarized in Tables 2–5 and Fig. 2.

3.2.1. CO_2 adsorption on T_{Co_3Cu}

A_{1_1} is the CO_2 adsorption configuration on supported Co_3Cu at the bridge-site, shown in Fig. 2a. In A_{1_1}, CO_2 is distorted almost symmetrically and bound at the Co_1–Cu_4 bridging site. Both Co_1–C (O) and Cu_4–C (O) bonds are formed. The adsorbed CO_2 is bent with the C–O bond being lengthened to 1.24–1.26 Å and the O–C–O angle being decreased to 142°. Consistent with our previous work, the adsorption led to a partially activated CO_2. The adsorption energy of CO_2 in A_{1_1} is −0.61 eV. The adsorption of CO_2 on another bridge site, Co_2–Cu_4, was found to have a similar stability and a similar

Table 5
Adsorption energies and structural parameters of CO_2 adsorbed on Co_4 (O^s labels the surface hydroxyl O atom).

	Co_4	ΔE_{ad} (eV)	$O^{a(b)}$…H–O^s (Å)	Adsorption site	C–O^a, C–O^b (Å)	∠O–C–O (°)
Mode 1	O1_1	−1.02	No	Co_1–Co_3	1.25, 1.26	140.8
	O1_2	−1.02	No	Co_2–Co_3	1.27, 1.25	139.6
Mode 2	O2_1	−0.97	1.62	Co_1–Co_2	1.24, 1.32	133.4
	O2_1′	−0.65	No	Co_1–Co_2	1.24, 1.27	137.2
	O2_2	−0.96	1.59	Co_1	1.21, 1.33	136.7
	O2_2′	−0.73	No	Co_1	1.21, 1.29	141.8
	O2_3	−0.89	1.62	Co_1	1.21, 1.30	138.8
	O2_3′	−0.74	No	Co_1	1.21, 1.28	143.6
Mode 3	O3_1	−1.56	1.60	Protonated	1.29, 1.33	115.2
	O3_2	−1.66	1.55	Protonated	1.27, 1.41	119.6

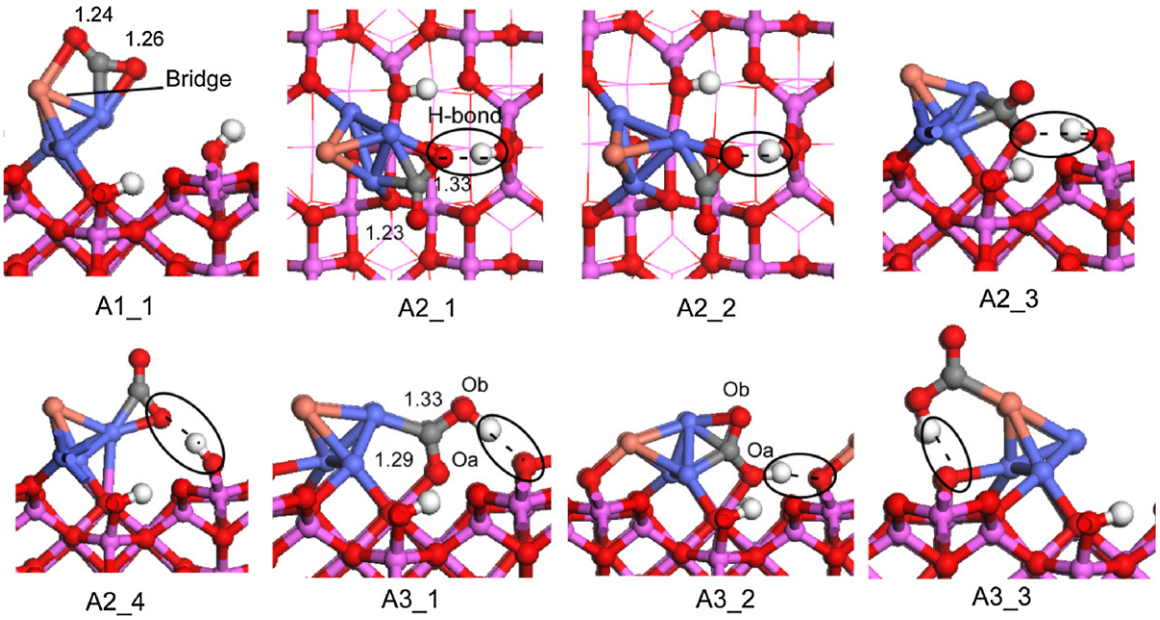

Fig. 2. Structure of CO_2 adsorption configurations on T_{Co_3Cu}. A_{1_1} (Mode 1); A_{2_1}, A_{2_2}, A_{2_3}, A_{2_4} (Mode 2); and A_{3_1}, A_{3_2}, A_{3_3} (Mode 3). Bond lengths are in Å (A_{2_1}, A_{2_2} and A_{2_4} show top views and others show side views).

stretched C–O bond to those in A_{1_1}. The results of Bader charge analysis for all CO_2 adsorption configurations on both Co_3Cu and $CoCu_3$ are summarized in Table 4. In A_{1_1}, CO_2 has a negative charge of −0.99 e, whereas the cluster has a positive charge of 0.78 e, indicating that CO_2 acts as a Lewis acid and accepts electron density mainly from the cluster.

Several Mode-2 configurations were located at the cluster–oxide interface. In A_{2_1}, CO_2 is bound at interfacial Co_1–Co_2 bridge site and coordinates with two metal atoms. The C–O bonds are stretched asymmetrically (1.23, 1.33 Å) with one O atom of CO_2 forming a hydrogen bond with the surface hydroxyl. The CO_2 molecular plane lay almost parallel to the cluster basal plane. The adsorption energy of CO_2 in A_{2_1} is −0.85 eV. The second interfacial configuration, A_{2_2}, is similar to A_{2_1}, but CO_2 only coordinates with the Co_1 atom via a mixed C and O coordination. Compared with the similar structure that has no H-bond, $A_{2\_2'}$, the extra stability contributed from hydrogen bonding accounts for 0.21 eV. We would point out that the adsorbed CO_2 becomes further distorted in A_{2_1} and A_{2_2} in the presence of hydrogen bonding. As we demonstrated later in the MD simulations, the single metal coordinated configuration is in fact very stable. The adsorbed CO_2 can rotate along the Co_1–O···H axis almost freely, leading to the local minima. A_{2_3} is another stable interfacial structure. In this structure, CO_2 coordinates via multiple cluster and surface sites, forming two Co–C bonds, one Co–O bond, and one O–Al_{4c} bond as well as a hydrogen bond. In A_{2_3}, CO_2 becomes more activated, commensurate with a further lengthened C–O bond and an even smaller O–C–O angle. All interfacial configurations are stabilized by the hydrogen bonding interactions and have similar stability.

In addition to the CO_2 adsorption configurations stabilized by hydrogen bonding at the cluster–support interface, a proton from the surface hydroxyl can be transferred to the adsorbed CO_2, leading to the pronated configurations, such as A_{3_1}, A_{3_2} and A_{3_3}, shown in Fig. 2. The A_{3_1} and A_{3_2} configurations involve the cluster–support interface, where CO_2 binds both cluster metal atoms and surface Al_{4c}. The migration of proton to CO_2 causes the cluster and adsorbed CO_2 to rotate, resulting in a side of the tetrahedron lying on the surface. In A_{3_1}, CO_2 interacts with cluster and substrate via C–Co_1 and O–Al_{4c} bonds. Proton was transferred to the free O_b. While in A_{3_2}, proton migrates to the "frozen" O_a and CO_2 interacts with two Co atoms via multiple C/O–cluster coordinations. The migration of proton to the "frozen" O_a causes the metal cluster to rotate, resulting in the Cu–O bond formation. The adsorbed CO_2 in both A_{3_1} and A_{3_2} was distorted dramatically. The O–C–O angles decrease to 115° and 118°, much smaller than that of gas-phase CO_2 (180°) and other adsorption modes (∼140°). The atomic charge of protonated CO_2 is −1.33 e, indicating a very strong electron transfer from the cluster and surface to CO_2. The adsorptions of CO_2 in A_{3_1} and A_{3_2} are strongly exothermic, with an adsorption energy around ∼−1.40 eV. The adsorptions of CO_2 in these two protonated configuration are significantly stronger than that of all other adsorption configurations. In A_{3_3}, CO_2 only interacts with the copper atom via the on-top C–Cu bond. The proton transfer to adsorbed CO_2 did not cause significant changes in cluster structure. A_{3_3} is much less stable than other two protonated configurations, due mainly to the suppressed contribution from the surface acidic sites.

Selecting the interfacial A_{2_2} configuration as the starting structure, we performed constant temperature molecular dynamics (MD) simulations at 300 K and 500 K to examine the dynamical aspect of CO_2 adsorption on the supported metal catalysts. In the initial structure, the CO_2 molecular plane is nearly parallel to the basal plane of the Co_3Cu cluster. At 500 K, CO_2 was found to rotate around the Co–O_a···H axis almost freely while maintaining the hydrogen bonding O_a···H–O_s interaction. We selected an energetically favorable structure in which CO_2 is located at a position such that the CO_2 plane is nearly perpendicular to the Co_1–Co_2–Co_3 plane along the MD trajectory and allowed it to relax to a new minimum, A_{2_4}, as shown in Fig. 2. The adsorption energy of CO_2 in A_{2_4} is −0.83 eV, indicating that A_{2_4} has almost the same stability as other interfacial configurations. The transformation from A_{2_2} to A_{2_4} goes through a transition state A_{2_5}, which was obtained from the MD trajectory at 300 K. The barrier of the transition is 0.15 eV. Based on the MD simulation results, we conclude that the single metal coordinated interfacial structures, A_{2_2} and A_{2_4}, are rather stable CO_2 configurations.

These MD results also indicated that each activated CO_2 adsorption configuration is stabilized by an activated barrier higher than the adsorption energy. An simply estimation based on the binding energy of 0.82 eV and a pre-exponential of 10^{13} at 500 K would

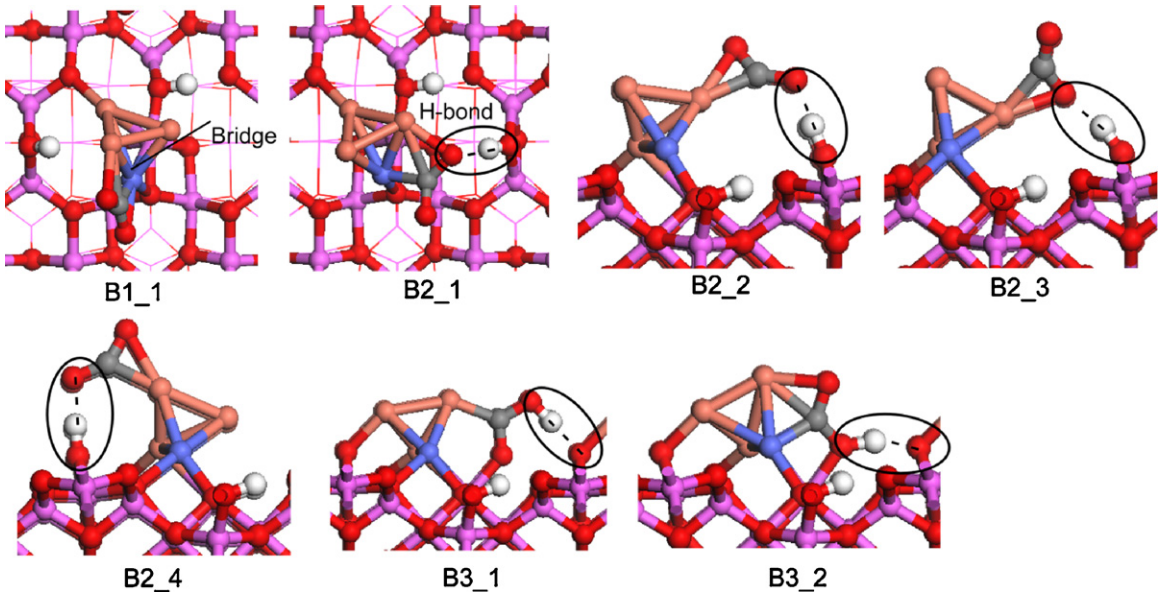

Fig. 3. Structures of CO_2 adsorption configuration on T_{CoCu_3}. B_{1_1} (Mode 1); B_{2_1}, B_{2_2}, B_{2_3}, B_{2_4} (Mode 2); and B_{3_1}, B_{3_2} (Mode 3).

yield a rate constant of 54,200 s^{-1}. A dynamics trajectory with such a rate constant will be almost certain to lead to desorption. The fact that none of the trajectories at temperatures below 500 K lead to CO_2 desorption indicates that the barriers of desorption for these adsorbed CO_2 are high than the adsorption energy.

Overall, the Co–Cu bridge site and interfacial Co_1 site are active sites for CO_2 adsorption and activation. This is consistent with the above discussed electronic structure of the supported Co_3Cu. In the supported Co_3Cu, Co_1 and Cu_4 atoms are both negatively charged and easily donate their electrons to CO_2. The extent of activation increases from the bridge site to interfacial site, and further to protonated structures. Table 4 summaries that the adsorbed CO_2 has a significant amount of negative charge whereas the cluster has nearly an equivalent amount of positive charge. The substrate surface is only slightly positive. Naturally, the protonated CO_2 is the most highly activated, corresponding to the longest C–O bond, smallest O–C–O angle and the largest amount of negative charges. These results confirm our previous observation that the hydroxylation of the γ-Al_2O_3 (1 1 0) surface enhances CO_2 activation [30].

In addition, we observe that the cluster–support interaction creates more active sites on the supported cluster through electron transfer and charge re-distribution, which further affect the activity of the supported catalysts. We found that in the interfacial configuration (Mode 2), the single metal coordinated configuration (A_{2_2} and A_{2_4}) and bi-metal coordinated configuration (A_{2_1}) have the similar stability. Similar observations occur in the corresponding protonated configurations (A_{3_1} and A_{3_2}). These results suggested a strong binding interaction of CO_2 on Co.

3.2.2. CO_2 adsorption on T_{CoCu_3}

Next we examined CO_2 adsorption on the supported $CoCu_3$ cluster. Similarly, the adsorption configurations of three adsorption modes are found, as summarized in Table 3 and Fig. 3. In B_{1_1}, CO_2 is bound at Co_2–Cu_4 bridge and symmetrically distorted. The calculated adsorption energy of CO_2 is −0.68 eV. B_{2_1} is the bi-metal coordinated configuration at the interfacial Cu_1–Co_2 bridge, in which CO_2 binds Cu_1 and Co_2 atoms by multiple C and O coordination. CO_2 is distorted asymmetrically and its plane is parallel to the basal plane of cluster. The CO_2 adsorption energy in B_{2_1} is −1.04 eV, much larger than that of B_{1_2}. Several single-metal coordinated interfacial configurations B_{2_2}, B_{2_3} and B_{2_4} were obtained, including CO_2 binding at the interface Cu_1 atom or at top vertex Cu_4 atom. The CO_2 adsorption energies of these single metal coordinated interface configurations are in the range of −0.11 to 0.46 eV, much smaller than that of bi-metal interface configuration B_{2_1} and the bridge-site configuration B_{2_1}, showing a weaker interaction between CO_2 and the cluster-oxides. Accordingly, the stability of the protonated configurations exhibits the same trend. B_{3_1} and B_{3_2} are the single and bimetal coordinated protonated configurations, respectively. The adsorption energy of CO_2 in B_{3_1} is −1.24 eV, while it is −1.70 eV in B_{3_2}. This indicated that the bridge site involving Co is much more active for CO_2 adsorption than the single Cu site.

MD simulation at both 300 K and 500 K was carried out using B_{2_1} as the initial structure. The trajectory study shows that the adsorbed CO_2 just vibrates near its initial position and no desorption happens within the simulation time. The randomly selected structures from MD were optimized and always reached the initial structure B_{2_1}. This proves that B_{2_1} is a very stable structure and the Cu–C and Co–C coordinates are very robust, while B_{2_2} and B_{2_3} are less stable and cannot be obtained through trajectory study at 300 K. To get the single-metal coordinated configuration B_{2_2} and B_{2_3}, a high temperature (e.g. 500 K) is necessary to overcome the barrier to break Co–C bond. The MD simulation confirmed the strong binding of Co toward CO_2 obtained in the static calculations.

It is worth mentioning that the protonated configurations at the interface are still the most favored, while the site activity shows a big difference in comparison with T_{Co_3Cu} system. Contrary to the less substituted cluster, the interface bridge site where Co is present in $CoCu_3$ becomes the energetically favorable site for CO_2 adsorption. The interfacial single-metal coordination is unfavorable even with hydrogen bonding's assistance at the cluster–oxide interface. The site activity alteration is closely related to the affinity of Cu to CO_2, which is much weaker than that of Co. In following section we provide a detailed structural comparison to elucidate this difference.

3.2.3. CO_2 adsorption on T_{Co_4}

To understand the effect of Cu incorporation in the cobalt cluster on Co, we studied CO_2 adsorption and activation on the supported Co_4 cluster. The results were used as references for CO_2 interaction with the bimetallic clusters. Similar configurations to those explored in Co_3Cu and $CoCu_3$ systems were studied for the sup-

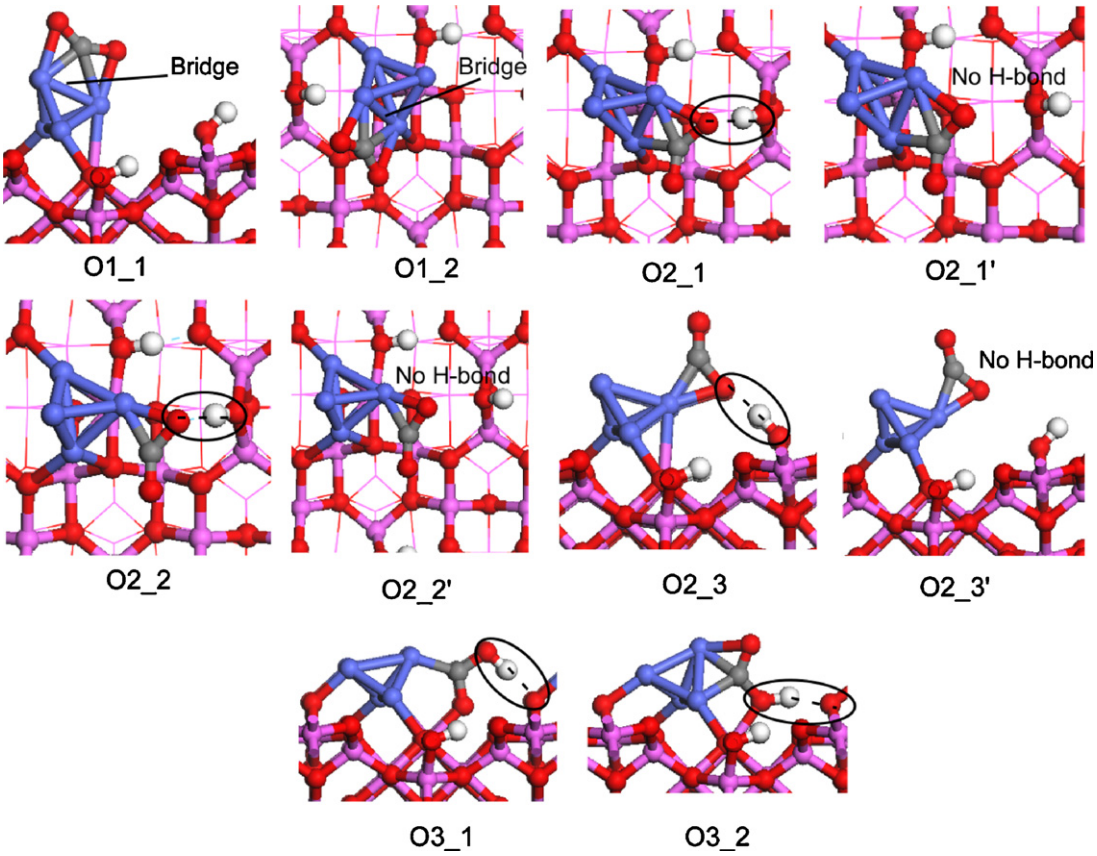

Fig. 4. Structure of CO_2 adsorption configurations on T_{Co_4}. Mode 1: O_{1_1} (side view) and O_{1_2} (top view); Mode 2: O_{2_1} and $O_{2\_1'}$ (top view), O_{2_2} and $O_{2\_2'}$ (top view), O_{2_3} and $O_{2\_3'}$ (side view); Mode 3: O_{3_1} and O_{3_2} (side view).

ported Co_4 cluster. The structural parameters for all configurations are tabulated in Table 5. Detailed structures of these configurations are provided in Fig. 4.

O_{1_1} and O_{1_2} are the Mode 1 configurations with CO_2 being adsorbed at bridging Co_1–Co_4 and Co_2–Co_4 sites, respectively. In Mode 1, CO_2 is distorted almost symmetrically and bound with two Co atoms through multiple Co–C and Co–O bonds. These sites are the energetically most favorable for CO_2 adsorption on the supported Co_4 cluster, with the adsorption energy being −1.02 eV. O_{2_1} is the interfacial configuration with the Co_1–Co_2 bridge site being involved, similar to A_{2_1} on T_{Co_3Cu} and B_{2_1} on T_{CoCu_3}. The other interfacial configurations include O_{2_2}, corresponding to A_{2_2}, and O_{2_3}, corresponding to A_{2_4}, in CO_2 adsorption on T_{Co_3Cu}. We also listed the structural parameters and the adsorption energies of CO_2 in the configurations that CO_2 interacts with cluster and surface in a similar mode but without forming hydrogen bonding. As shown in Table 5, the overall trend is that the interfacial configurations are less favorable than those formed at the bridge sites, although hydrogen bonding increases the stability by 0.15–0.32 eV. On the other hand, once the adsorbed CO_2 became protonated, their stabilities are enhanced greatly, making them, O_{3_1} and O_{3_2}, the most favorable configurations. The adsorption energies of CO_2 in O_{3_1} and O_{3_2} are −1.56, −1.66 eV, respectively.

Table 6 lists a detailed comparison of bond lengths of single-metal and bi-metal coordinated configurations. The Co–C and Co–O bonds in single-metal coordinated configurations are shorter than the corresponding bonds of the bi-metal coordination whereas the stabilities of these configurations are similar. These results suggest that the short Co–C and Co–O bonds in single-metal coordinated configurations provide similar binding strength to the multiple but longer Co–C and Co–O bonds in the bi-metal coordinated configurations.

3.3. *Effect of Cu substitution on CO_2 adsorption*

The above results indicate that incorporating Cu into the Co cluster definitely affects the interaction of CO_2 with the supported clusters, and the extent of the influence depends on the composition of the cluster. Our results clearly demonstrated that the favorable adsorption site for CO_2 varies as the amount of incorporated Cu changes. From Co_4 to Co_3Cu, and then to $CoCu_3$, the active sites for CO_2 adsorption changes from the bridge site on cluster to the interfacial sites, and specifically, the interfacial bridge site.

As we showed above, the vertex and interfacial metal atoms binding the substrate Al_{4c} site are negatively charged. Incorporating Cu reduces the electron donating ability of the cluster, thereby, resulting in a less positively charged cluster. This will in turn weaken the binding of the cluster toward CO_2. For example, the adsorption energy of CO_2 in the bridge site decreases from −1.02 eV in Co_4 to −0.60 eV and −0.68 eV in Co_3Cu and $CoCu_3$, respectively. Consequently, this changes the order of stability of different CO_2 adsorption modes, making the most stable bridging site in Co_4

Table 6
Bond lengths and adsorption energies of bi- and single-metal coordinated CO_2 adsorption configurations on γ-Al_2O_3 supported Co_4.

Bi-metal	O_{1_1}	O_{2_1}	O_{3_2}
Co–C (Å)	1.87, 2.17	1.97, 1.92	1.89, 1.89
Co–O (Å)	2.11, 2.03	2.02	2.12
ΔE_{ad} (eV)	−1.02	−0.97	−1.66
Single-metal	O_{2_2}	O_{2_3}	O_{3_1}
Co–C (Å)	1.81	1.87	1.86
Co–O (Å)	1.93	1.95	
ΔE_{ad} (eV)	−0.96	−0.89	−1.56

Table 7
Bond lengths and adsorption energies of bi- and single-metal coordinated CO_2 adsorption configurations on γ-Al_2O_3 supported Co_3Cu and $CoCu_3$.

Bi-metal coordination	On T_{Co_3Cu}		On T_{CoCu_3}	
	A_{2_1}	A_{3_2}	B_{2_1}	B_{3_2}
Co–C (Å)	2.02, 1.91	1.93, 1.84	1.84 (C–Co) 2.27 (C–Cu)	1.81 (C–Co) 2.19 (C–Cu)
Co–O (Å)	2.00	2.09	2.06 (O–Cu)	2.12 (O–Cu)
ΔE_{ad} (eV)	−0.85	−1.39	−1.04	−1.70

Single-metal coordination	A_{2_4}	A_{3_1}	B_{2_3}	B_{3_1}
Co–C (Å)	1.89	1.90	1.98 (C–Cu)	1.91 (C–Cu)
Co–O (Å)	1.95		2.04 (O–Cu)	
ΔE_{ad} (eV)	−0.83	−1.34	−0.11	−1.24

cluster not favorable any more in both Co_3Cu and $CoCu_3$. This is consistent with the fact that the electron donating ability of the transition metals decreases from the left to right in the periodic table and consistent with the previous study [31].

Table 7 compares the detailed geometry of the interfacial configurations formed on the supported Co_3Cu and $CoCu_3$. In supported Co_3Cu, the interfacial sites were not affected because Cu substitution took place at the top vertex site. As a result, the interfacial sites showed a similar activity toward CO_2 adsorption. The CO_2 adsorption energy is reduced slightly due to Cu incorporation. When more Cu was incorporated, as in $CoCu_3$, the Cu–C and Cu–O bonds at the single metal site became much longer than the Co–C and Co–O bonds at the interfacial bridge site, corresponding to the weak binding ability of Cu to CO_2. This resulted in the interfacial single metal site being the least favorable for CO_2 adsorption on supported $CoCu_3$.

Clearly, the complex formed from CO_2 adsorption at the cluster–support interface is controlled by composition and structural details. The correlation between the composition and interfacial structure provide us a means to manipulate the atomic structure at the interface by tuning catalyst composition. As indicated by the results in the present study, increasing the Cu composition to $CoCu_3$ forces Cu to the interfacial site, which affects the reactivity of the Co-based cluster. On the supported pure Co cluster, the symmetrically activated CO_2 species in the bridging Co–Co is the energetically favorable species. In the supported Co_3Cu, CO_2 activation at the interfacial sites becomes favorable, resulting in the asymmetrically activated CO_2 species. With more Cu incorporated, as in $CoCu_3$, the asymmetrically activated CO_2 species at the interfacial *bridge* site (bi-metal coordination) becomes favorable. These changes in active sites for CO_2 adsorption and activation due to Cu substitution may also alter reaction pathways and affect final product distribution. For example, the C-center of the asymmetrically activated CO_2 may be facile to direct hydrogenation while maintaining the dangling C–O bond, making oxygenate species (such as methanol) possible products in direct CO_2 hydrogenation.

4. Conclusion

Adsorption and activation of CO_2 on the γ-Al_2O_3 supported bimetallic Co–Cu clusters have been studied using DFT slab calculations. In particular, we examined the effect of substitution of Co by Cu in the supported metal cluster on the cluster's reactivity toward CO_2 adsorption and activation. On the basis of the results, we conclude:

(1) Adsorbed CO_2 on the γ-Al_2O_3 supported Co_4, Co_3Cu, and $CoCu_3$ is highly activated, indicated by the elongated C–O bond(s) and reduced O–C–O angle. Finite temperature molecular dynamics simulations show that each CO_2 adsorption configuration is stabilized by an activation barrier higher than the corresponding adsorption energy.
(2) The active site for CO_2 adsorption and activation varies as the composition of the cluster changes. On supported Co_4, CO_2 is activated almost symmetrically at the Co–Co bridge site away from the interface. In both supported Co_3Cu and $CoCu_3$, CO_2 activation occurs at the cluster–support interface, resulting in asymmetrically activated CO_2.
(3) The presence of surface hydroxyls helps to stabilize the adsorbed CO_2 species by either hydrogen bonding or protonating CO_2. The hydrogen bonding stabilizes the structure by ∼0.2 eV whereas protonation has a much pronounced effect.

Acknowledgements

This work is supported in part by the Illinois Clean Coal Institute. We also acknowledge the support of the Molecular Science Computing Facility in the William R. Wiley Environmental Molecular Science Laboratory (EMSL), located at Pacific Northwest National Laboratory (PNNL).

References

[1] M.M. Halmann, M. Steinberg, Greenhouse Gas Carbon Dioxide Mitigation: Science and Technology, CRC Press, Boca Raton, 1999.
[2] C.S. Song, Catal. Today 115 (2006) 2.
[3] A.D. Ballarini, S.P. de Miguel, E.L. Jablonski, O.A. Scelza, A.A. Castro, Catal. Today 107–108 (2005) 481.
[4] E. Ruckenstein, H.Y. Wang, J. Catal. 205 (2002) 289.
[5] Y.H. Hu, Catal. Today 148 (2009) 206.
[6] K.M.K. Yu, C.M.Y. Yeung, S.C. Tsang, J. Am. Chem. Soc. 129 (2007) 6360.
[7] Q.L. Tang, Q.J. Hong, Z.P. Liu, J. Catal. 263 (2009) 114.
[8] Z.S. Hong, Y. Gao, J.F. Deng, K.N. Fan, Catal. Lett. 82 (2002) 37.
[9] Y.P. Zhang, J.H. Fei, Y.M. Yu, X.M. Zheng, Energy Convers. Manage. 47 (2006) 3360.
[10] K. Klier, Adv. Catal. 31 (1982) 243.
[11] I.A. Fisher, A.T. Bell, J. Catal. 172 (1997) 222.
[12] J. Weigel, R.A. Koppel, A. Baiker, A. Wokaun, Langmuir 12 (1996) 5319.
[13] S. Krishnamoorthy, A.W. Li, E. Iglesia, Catal. Lett. 80 (2002) 77.
[14] S.Z. Li, A.W. Li, S. Krishnamoorthy, E. Iglesia, Catal. Lett. 77 (2001) 197.
[15] P.S. Sai Prasad, J.W. Bae, K.W. Jun, K.W. Lee, Catal. Surv. Asia 12 (2008) 170.
[16] G. Kishan, M.W. Lee, S.S. Nam, M.J. Choi, K.W. Lee, Catal. Lett. 56 (1998) 215.
[17] R.W. Dorner, D.R. Hardy, F.W. William, B.H. Davis, H.D. Willauer, Energy Fuels 23 (2009) 4190.
[18] J.R. Anderson, M. Boudart, Catalyst: Science and Technology, vol. 1, Springer-Verlag, Berlin, 1984.
[19] K. Pansanga, N. Lohitharn, A.C.Y. Chien, E. Lotero, J. Panpranot, P. Praserthdam, J.G. Goodwin Jr., Appl. Catal. A 332 (2007) 130.
[20] W.S. Ning, N. Koizumi, H. Chang, T. Mochizuki, T. Itoh, M. Yamada, Appl. Catal. A 312 (2006) 35.
[21] G. Jacobs, M.C. Ribeiro, W.P. Ma, Y.Y. Ji, S. Khalid, P.T.A. Sumodjo, B.H. Davis, Appl. Catal. A 361 (2009) 137.
[22] C.J. Bertole, C.A. Mims, G. Kiss, J. Catal. 221 (2004) 191.
[23] T.K. Das, G. Jacobs, P.M. Patterson, W.A. Corner, J.L. Li, B.H. Davis, Fuel 82 (2003) 805.
[24] N. Tsubaki, S.L. Sun, K. Fujimoto, J. Catal. 199 (2001) 236.
[25] D. Schanke, S. Vada, E.A. Blekkan, A.M. Hilmen, A. Hoff, A. Holmen, J. Catal. 156 (1995) 85.
[26] M. Ronning, D.G. Nicholson, A. Holmen, Catal. Lett. 72 (2001) 141.
[27] H.J. Freund, R.P. Messmer, Surf. Sci. 172 (1986) 1.
[28] X. Ding, L. De Rogatis, E. Vesselli, A. Baraldi, G. Comelli, R. Rosei, L. Savio, L. Vattuone, M. Rocca, P. Fornasiero, F. Ancilotto, A. Baldereschi, M. Peressi, Phys. Rev. B 76 (2007) 195425.
[29] J.A. Rodriguez, Langmuir 4 (1988) 1006.

[30] Y.-X. Pan, C.-J. Liu, Q. Ge, Langmuir 24 (2008) 12410.
[31] Y.-X. Pan, C.-J. Liu, T.S. Wiltowski, Q. Ge, Catal. Today 24 (2009) 68.
[32] Y.-X. Pan, C.-J. Liu, Q. Ge, J. Catal. 272 (2010) 227.
[33] T. Kakumoto, T. Watanabe, Catal. Today 36 (1997) 39.
[34] M. Digne, P. Sautet, P. Raybaud, P. Euzen, H. Toulhoat, J. Catal. 226 (2004) 54.
[35] G. Kresse, J. Hafner, Phys. Rev. B 48 (1993) 13115.
[36] G. Kresse, J. Furthmueller, Phys. Rev. B 54 (1996) 11169.
[37] G. Kresse, D. Joubert, Phys. Rev. B 59 (1999) 1758.
[38] P.E. Blöchl, Phys. Rev. B 50 (1994) 17953.
[39] J.P. Perdew, K. Burke, M. Ernzerhof, Phys. Rev. Lett. 77 (1996) 3865.
[40] H.J. Monkhorst, J.D. Pack, Phys. Rev. B 13 (1976) 5188.
[41] R.F.W. Bader, Acc. Chem. Res. 18 (1985) 9.
[42] G. Henkelman, A. Arnaldsson, H. Jonsson, Comput. Mater. Sci. 36 (2006) 354.